Chapter 2
Thermodynamic and Kinetic Properties of Molecular Beacons

Lu Peng and Weihong Tan

Abstract Molecular beacons are widely used for detection of nucleic acids both in vitro and in vivo. Compared with linear probes, molecular beacons have shown enhanced sensitivity and specificity primarily due to their stem–loop hairpin structures. The hairpin structures bring new considerations on thermodynamics and kinetics for designing of nucleic acid probes. This chapter has been designed to provide a better understanding of structure–performance relationship of molecular beacons based on analysis of their thermodynamic and kinetic properties. The conformational fluctuations of molecular beacons are discussed concerning the stability and kinetics of the hairpin-coil transformation. In the presence of target nucleic acids, molecular beacons hybridize with targets to form duplex complexes. We analyzed the theoretical models and the relevant parameters used to describe the hybridization reactions. Furthermore, studies on strategies for optimization of molecular beacon performance are summarized. The systematic analysis of studies about thermodynamic and kinetic properties of molecular beacons allows for sophisticated design of better molecular beacons for specific purposes.

2.1 Introduction

Molecular beacons are designed with a target-specific hybridization domain positioned between two short self-complementary sequences [1]. In the absence of target, the intramolecular hybridization reaction between the self-complementary

L. Peng (✉)
Department of Chemistry, University of Florida, Gainesville, FL 32611, USA
e-mail: lupeng@ufl.edu

W. Tan
Department of Biomedical Engineering and Department of Chemistry, Hunan University, Changsha, P.R. China

Department of Chemistry, University of Florida, Gainesville, FL, USA
e-mail: tan@chem.ufl.edu

C.J. Yang and W. Tan (eds.), *Molecular Beacons*, DOI 10.1007/978-3-642-39109-5_2,

domains generates a stem–loop hairpin structure and brings the fluorophore into close proximity with the quencher, resulting in fluorescence quenching. For any applications using molecular beacons, the best probe performance depends on design optimization. For example, while high specificity is required to identify single nucleotide polymorphisms (SNP), real-time study of transient RNA expression in vitro requires fast hybridization kinetics [2]. Thus, knowledge of the thermodynamics and kinetics of molecular beacons is a design prerequisite. During the last several years, many studies have addressed the conformational fluctuation of molecular beacons and their interactions with targets from the perspective of thermodynamics and kinetics, and in this chapter, these properties will be discussed.

2.2 Conformational Fluctuations of Molecular Beacons

Molecular beacons represent a class of hairpin nucleic acid probes with stem–loop structures. Although the signaling groups (fluorophores and quenchers) report hybridization events, the performance and function of molecular beacons as hybridization probes are essentially determined by the thermodynamic and kinetic properties of hairpin structures. Hairpins are the dominant secondary structure element in RNA. Certain sequences possess exceptionally high thermodynamic stability with the ability to determine such biological functions as enzymatic and anti-RNase activity.

The hairpin structures of molecular beacons are not static. They fluctuate between different conformations, particularly the open and closed states, as shown in Fig. 2.1 [3]. As a consequence of base pairing in the hairpin's stem region, the closed state has low enthalpy. On the other hand, the open state has high enthalpy by the large number of configurations that can be achieved by a single-stranded DNA (ssDNA). Thus, while the transition from the closed state to the open state requires an energy force great enough to break all the base pairs, collision of the two hairpin arms is necessary to close the hairpin, followed by the nucleation and the propagation of base pairing in the stem.

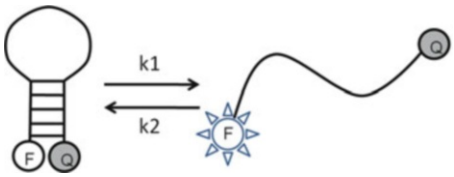

Fig. 2.1 Sketch of the conformational fluctuation of a DNA molecular beacon. The molecular beacon fluctuates between open and closed states with the rate constants k_1 and k_2. The fluorophore (F) and the quencher (Q) are covalently attached to the two arms. Fluorescence is quenched in the closed state; however, upon target recognition, the hairpin structure is opened, and the MB emits fluorescence

2.2.1 Thermodynamics of Hairpins

Enthalpy is a thermodynamic potential, measuring the total energy of a thermodynamic system. The total enthalpy, H, of a system cannot be measured directly. Thus, change in enthalpy, ΔH, is a more useful quantity than its absolute value. ΔH of a system is equal to the sum of nonmechanical work done on it and the heat supplied to it. Entropy is the thermodynamic property toward equilibrium/average/homogenization/dissipation. That is, the hotter, more dynamic areas of a system lose heat/energy, while cooler areas (e.g., space) get warmer/gain energy. Entropy of a system can be measured to determine the energy not available for work in a thermodynamic process.

Thermodynamic parameters of hairpins, including enthalpies and entropies, are revealed by melting studies [4–6]. In a typical experiment, the unfolding heat of a hairpin is measured with a differential scanning calorimeter (DSC). A DNA solution is scanned against a buffer solution within a certain temperature range, normalized by the heating rate and a buffer versus buffer scan subtracted and normalized by the effective number of moles used. Integration of the resulting curve, $\int \Delta C_p \mathrm{d}T$, yields model-independent enthalpy, ΔH_{cal}. Change in entropy, ΔS_{cal}, is obtained by a similar integration, $\int (\Delta C_p/T)\mathrm{d}T$, and checked against a standard relationship for intramolecular transitions: $\Delta S_{cal} = \Delta H_{cal}/T_M$. In the measurement of these terms, it is assumed that the duplex and random-coil states have similar heat capacities. The free energy at any temperature T is obtained by the Gibbs relationship: $\Delta G^{\circ}_{cal}(T) = \Delta H_{cal} - T\Delta S_{cal} = \Delta H_{cal}\,(1 - T/T_M)$ [7].

The free energy of a hairpin can be broken into two parts: the free energy of forming a loop closed by a single base pair and the free energy for the base-paired stem of the hairpin. The free energy of the stem can be analyzed with the nearest-neighbor model for both stacking and base pairing [5, 8]. Therefore, the free energy for loop formation is determined by subtracting the free energy for stem from those measured free energy for the hairpin from optical or DSC melting studies.

2.2.2 Factors Affecting the Stability of Hairpins

The stability of a hairpin is characterized by its melting temperature. At the melting point, the change in Gibbs free energy (ΔG) of the material is zero, but the enthalpy (H) and the entropy (S) of the material are increasing (ΔH, $\Delta S > 0$). The melting phenomenon happens when the Gibbs free energy of the liquid becomes lower than the solid for that material. Accordingly, the relationship between melting temperature and Gibbs free energy is shown in the following equation: $\Delta G^{\circ}_{cal}(T) = \Delta H_{cal} - T\Delta S_{cal} = \Delta H_{cal}\,(1 - T/T_M)$. The factors that contribute to the difference in free energy are also responsible for the stability of hairpins.

The effect of stem structures on the stability of hairpins can be explained by the nearest-neighbor model. Briefly, the *k*-nearest-neighbor (*k*-NN) algorithm is among the simplest of all machine learning algorithms: an object is classified by a majority vote of its neighbors, with the object being assigned to the class most common among its *k*-nearest neighbors (*k* is a positive integer, typically small). If $k = 1$, then the object is simply assigned to the class of its nearest neighbor. In our case, the interaction between bases on the two arms of hairpins depends somewhat on the neighboring bases. Instead of treating a DNA duplex as a string of interactions between base pairs, the nearest-neighbor model treats a DNA helix as a string of interactions between "neighboring" base pairs [9]. As such, the enthalpy (ΔH°), entropy (ΔS°), and free energy (ΔG°) of duplex annealing in the stem region are predicted by the nearest-neighbor method and thermodynamic parameters [9, 10]. Stem length and the identity of the nearest-neighbor bases determine the stability of the stem. The arrows in the example below indicate the nearest-neighbor interactions in the stem of a hairpin.

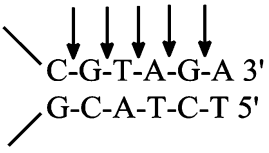

The free energy of forming the stem at 37 °C, ΔG°_{37} (stem), is represented as

$$\begin{aligned}\Delta G^\circ_{37}(\text{stem}) = {} & \Delta G^\circ_{37}(\text{CG initiation}) + \Delta G^\circ_{37}\left(\frac{\text{CG}}{\text{GC}}\right) + \Delta G^\circ_{37}\left(\frac{\text{GT}}{\text{CA}}\right) \\ & + \Delta G^\circ_{37}\left(\frac{\text{TA}}{\text{AT}}\right) + \Delta G^\circ_{37}\left(\frac{\text{AG}}{\text{TC}}\right) + \Delta G^\circ_{37}\left(\frac{\text{GA}}{\text{CT}}\right) \\ & + \Delta G^\circ_{37}(\text{AT initiation}) \end{aligned} \tag{2.1}$$

The first term, ΔG°_{37} (CG initiation), represents the free energy of the first base pair, CG, in the absence of a nearest neighbor. The second term, ΔG°_{37} (CG/GC), includes both the free energy of base pairing, GC, and the stacking interaction of this base pair with the previous base pair, CG. The remaining terms are defined in a similar manner. As a general rule, the free energy of stem formation of a hairpin is calculated by the equation below:

$$\Delta G^\circ_{37}(\text{stem}) = \Delta G^\circ_{37}(\text{initiation}) + \sum_{i=1}^{10} n_i \Delta G^\circ_{37}(i) \tag{2.2}$$

Based on Gibbs relationship, ΔG°(stem) is also given by

$$\Delta G^\circ_{37}(\text{stem}) = \Delta H^\circ(\text{stem}) - T\Delta S(\text{stem}) \tag{2.3}$$

Table 2.1 Nearest-neighbor parameters for DNA/DNA duplexes in 1 M NaCl

Nearest-neighbor sequence (5′-3′/3′-5′)	ΔH° kJ/mol	ΔS° J/(mol · K)	ΔG° kJ/mol
AA/TT	−33.1	−92.9	−4.26
AT/TA	−30.1	−85.4	−3.67
TA/AT	−30.1	−89.1	−2.50
CA/GT	−35.6	−95.0	−6.12
GT/CA	−35.1	−93.7	−6.09
CT/GA	−32.6	−87.9	−5.40
GA/CT	−34.3	−92.9	−5.51
CG/GC	−44.4	−113.8	−9.07
GC/CG	−41.0	−102.1	−9.36
GG/CC	−33.5	−83.3	−7.66
Terminal A-T base pair	9.6	17.2	4.31
Terminal G-C base pair	0.4	−11.7	4.05

Reprinted with the permission from Ref. [9]. Copyright 1998, National Academy of Sciences, USA

Values of ΔH° and ΔS° have been predicted by nearest-neighbor method for all the ten possible pairs of nearest-neighbor interactions, as given in Table 2.1, along with the values of ΔG°_{37}. The parameters associated with the ten groups of neighbors shown in Table 2.1 are determined from melting points of short oligonucleotide duplexes [9]. The parameters calculated with the nearest-neighbor method agree well with experimental results.

Besides the stem structures, the loop structure, including loop sequences and loop length, also plays an important role in the stability of hairpins. Traditionally, the stem of a nucleic acid hairpin is regarded as a highly structured helix and the loop as a disordered coil. The thermodynamic stability of hairpins was attributed to the stem sequence. Single-stranded loops were assumed to destabilize the folded hairpin structure in an entropic manner based on the length of loops [11]. Thus, DNA hairpins with loop length of four to five residues were found to have maximum stability [12, 13], whereas early studies showed that RNA hairpin loops with six to seven nucleotides have highest stability [14]. These results correlated well with a simple structural principle [13]: that the steric hindrance effect for the folding of hairpin is mainly caused by the fact that the loop bridges the gap between the two complementary opposite sides of the stem. The enthalpy of DNA hairpin formation reaches a minimal value for loops of four to five nucleotides. On the other hand, the melting temperature decreases at increasing loop size based on the unfavorable entropy effect of loop formation [13]. Loop sequence has less effect on loop stability than its length. For DNA hairpins sharing the same stem, but with different 4-base loops, the order of stability was T loop > C loop > G loop > A loop, and the largest difference in melting temperature was 5–6 °C between the most stable T loop and least stable A loop [15].

In addition to the effect of stem and loop structures on the stability of hairpins, metal ions, such as Na^+ and Mg^{2+} ions, are also essential in stabilizing the

folded hairpins through electrostatic interactions. Salt-dependent correction terms for the thermodynamic parameters of nucleic acid hybridization have been obtained from both experimental data [16, 17] and theoretical modeling [18, 19]. The salt dependence of hairpin stability has also been addressed [20].

2.2.3 Kinetics of Conformational Fluctuations of Hairpins

Kinetics studies have been conducted on the process of double-helix formation of RNA and DNA [21, 22]. Because of the fast kinetics of helix formation, a rapid kinetics approach is required. Using a laser or a capacitor to rapidly heat the water, the temperature jump (T-jump) method has been widely employed [23–25]. Controlled by a thermostatted bath, temperature jump is a perturbation method in which the system starts at equilibrium at a certain temperature (T_{init}) and ends at equilibrium at a higher temperature (T_{final}) [26]. Methods of duplex detection include absorbance, as well as fluorescence, optical activity, scattering, and conductivity. The relaxation of the system (τ) going from T_{init} to T_{final} is observed. In the open-to-closed transition of hairpin,

$$\text{coil} \underset{k_{-1}}{\overset{k_1}{\rightleftarrows}} \text{hairpin}$$

the observed relaxation rate, $1/\tau$, is given by the equation [3]

$$\frac{1}{\tau} = k_1 + k_{-1} \tag{2.4}$$

To extract k_1 and k_{-1} from τ, the equilibrium constant for the helix–coil transition, it is necessary to determine K by the optical or melting method. The relationship is given by:

$$K = \frac{k_1}{k_{-1}} \tag{2.5}$$

Combining Eqs. (2.4) and (2.5), both closing and opening rate constants can be solved. By study of fluorescence quenching using fluorescence correlation spectroscopy (FCS), it was found that closing rates depend on the sequence and length of the loop [3]. The results were confirmed by the laser T-jump method [23] and agreed well with a semiflexible polymer model [25]. A deviation from Arrhenius kinetics, i.e., the rate of a chemical reaction, was found in studies of Förster resonance energy transfer (FRET) fluctuations in DNA hairpins [27, 28]. Here, while the opening rate depends on the unzipping energy of the hairpin, it is essentially independent of loop characteristics, irrespective of loop size, sequence, and NaCl concentration [3].

2.3 Hybridization Thermodynamics and Kinetics of Molecular Beacons

2.3.1 Thermodynamics

Hybridization assays with sequence-specific oligonucleotide probes are commonly used techniques for the identification of complementary strands and the detection of genetic mutations and polymorphisms. However, linear oligonucleotide probes have limited abilities in cases where detection of single nucleotide polymorphism (SNP) is required. Specifically, an energy penalty is applied for any mismatched base pairs which destabilize the double helix. However, if the duplex is sufficiently long, the free energy penalty from a single-base mismatch becomes negligible [29]. Therefore, the mismatched base pair only minimally affects the stability of the resulting duplex. It is often necessary to use proteins or other chemicals to assist in the identification of mismatched base pairs [30, 31].

During the last two decades, the emergence of molecular beacons, which are stem–loop probes, has greatly improved our capabilities in the analytical, biochemical, and biomedical fields. Compared with linear nucleic acid probes, one of the most attractive features of molecular beacons is enhanced specificity by the ability to form a stem–loop structure. The hairpin structure enables molecular beacons to discriminate between targets with even a single nucleotide. The competition between the formation of unimolecular hairpin and the probe–target hybridization reduces the probability of mismatched hybridization events from the relatively low stability [32–34].

2.3.1.1 Determination of Thermodynamic Parameters

As shown in Fig. 2.2, linear nucleic acid probes have two possible states with their targets: linear probe–target duplex and random coil. In contrast, molecular beacons in solution with their targets can have at least three distinct states: molecular beacon–target duplex (phase 1), stem–loop hairpin (phase 2), and random coil (phase 3) [2, 35].

Following Bonnet et al. [36] and Tsourkas et al. [2], the dissociation constant K_{2-3} corresponding to the transition between stem–loop hairpin and random coil is given by:

$$K_{2-3}(\theta) = \left(\frac{F-\beta}{\gamma-F}\right) \tag{2.6}$$

where F is the fluorescence intensity at a given temperature θ, β is the fluorescence of molecular beacons in the hairpin form (obtained at low temperatures, such as 10 °C), and γ is the fluorescence of molecular beacons in the random-coil form (obtained at high temperatures, such as 80 °C) in the absence of targets [36]. Based

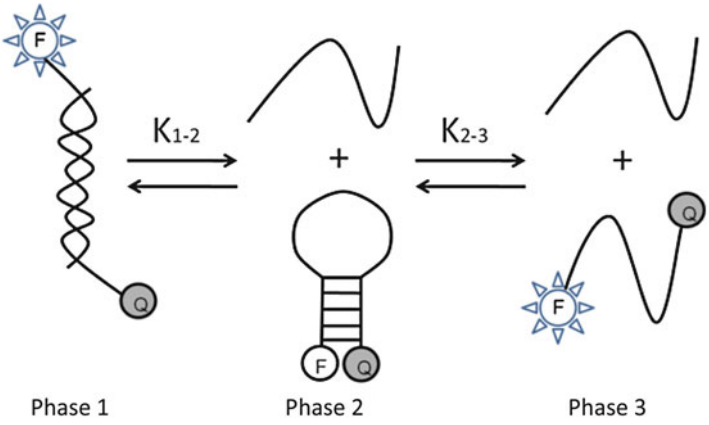

Fig. 2.2 Phase transitions of molecular beacons with targets in solution. Phase 1: fluorescent molecular beacon–target duplex; phase 2: nonfluorescent stem–loop hairpin; and phase 3: fluorescent random coil

on the Gibbs relationship,

$$\Delta G^{\circ}_{2-3} = \Delta H^{\circ}_{2-3} - \theta \Delta S^{\circ}_{2-3} \tag{2.7}$$

and the relationship between free energy and equilibrium constant,

$$\Delta G^{\circ}_{2-3} = -RTlnK_{2-3}(\theta) \tag{2.8}$$

fluorescence and temperature can be correlated by

$$Rln\left(\frac{F-\beta}{\gamma-F}\right) = -\Delta H^{\circ}_{2-3}\frac{1}{\theta} + \Delta S^{\circ}_{2-3} \tag{2.9}$$

where R is the gas constant (1.9872 cal mol^{-1} K^{-1}), T is the temperature in Kelvin, and ΔH_{2-3} and ΔS_{2-3} are the changes in enthalpy and entropy in the transition, respectively, which are determined by fitting the fluorescence–temperature data into a straight line using this equation.

The thermodynamic parameters for the transition from a molecular–target duplex (phase 1) to a stem–loop hairpin (phase 2), ΔH°_{1-2} and ΔS°_{1-2}, were determined by fluorescence measurements of the thermal denaturation profiles in the presence of targets at different concentrations. At the melting temperature of the duplex (θ_{m}), the concentration of molecular beacons in the hairpin form (M_{hairpin}) equals the concentration of the probe–target duplex (MT). Therefore, based on the equation

$$K_{1-2} = \frac{[M_{\mathrm{hairpin}}][T]}{[MT]} \tag{2.10}$$

$K_{1-2} = T_m = T_0 - 0.5M_0$, where T_m is the concentration of free target and T_0 and M_0 are the initial concentrations of targets and molecular beacons, respectively. The thermodynamic parameters ΔH°_{1-2} and ΔS°_{1-2} can be determined by fitting the concentration-melting temperature data into a straight line using this equation, which establishes the relationship between melting temperature and the thermodynamic parameters, ΔH°_{1-2} and ΔS°_{1-2}:

$$RlnK_{1-2}(\theta_m) = Rln(T_0 - 0.5M_0) = -\Delta H^\circ_{1-2}\frac{1}{\theta_m} + \Delta S^\circ_{1-2} \tag{2.11}$$

The dissociation constant K_{1-2} characterizing the transition between molecular beacon–target duplex and the stem–loop hairpin can be determined from the fluorescence data obtained by the melting measurements of molecular beacons in the presence of target [36], by the equation

$$K_{1-2}(T) = \frac{(\alpha - F)T_0}{(F - \beta) + (F - \gamma)K_{2-3}} \tag{2.12}$$

where α is the fluorescence intensity of molecular beacon–target duplex at low temperatures such as 10 °C, and F and β are the same as above mentioned in Eq. (2.6).

Equilibrium states of molecular beacons in the presence of targets can be significantly influenced by the probe (loop) length. For example, Tsourkas et al. found that both ΔH°_{1-2} and ΔS°_{1-2} increase when probe length increases from 17 to 19 bases for a molecular beacon with a five-base stem. It was also found that the stem length of a molecular beacon had greater effect on its equilibrium state than the loop length [2, 37]. The effect of mismatched base pairs on the equilibrium states of molecular beacons was also studied [2, 36]. The target with single-base mismatches showed a less favorable binding with molecular beacons. Furthermore, a centrally positioned mismatch had a greater impact on equilibrium than a terminal mismatch in the probe domain of a molecular beacon [2, 36].

2.3.1.2 Melting Temperature

The stability of probe–target duplex is expressed in terms of melting temperature. To demonstrate the effect of molecular beacon structure on melting behavior of the probe–target duplex, the melting temperature was studied by varying the loop and stem structures. Tsourkas et al. found that melting temperature increased with probe length. Stem length also had the same effect on melting temperature [2]. For three molecular beacons, each having 17 bases in the loop domain, the melting temperature decreased by 7.8 °C when the stem length was increased from four to six. Moreover, when probe length was shorter, stem length was observed to have a relatively greater impact on melting temperature.

Table 2.2 Melting temperatures for the dissociation of a perfectly complementary probe–target duplex (first entry), probe–target duplexes containing different mismatched base pairs at the same position (next three entries), and probe–target duplexes containing the same mismatched base pair at different positions (last nine entries)

Mismatch	Position (n)	θ_m (°C)
T-A	0	42
A-A	0	27
C-A	0	23
G-A	0	28
G-A	−4	30
G-A	−3	29
G-A	−2	30
G-A	−1	29
G-A	0	28
G-A	+1	29
G-A	+2	29
G-A	+3	29
G-A	+4	31

Reprinted with the permission from Ref. [36]. Copyright 1999, National Academy of Sciences, USA

The presence of mismatched bases also has a significant effect on the melting temperature of molecular beacon–target duplex. As shown by Bonnet et al. in Table 2.2, single-base mismatches greatly reduce the melting temperature of the probe–target duplex by more than 10 °C [36]. However, the position of the single-base mismatches did not have any impact on the stability of the probe–target duplex, which was consistent with the prediction made using an all-or-none mechanism whereby an action potential occurs fully or not at all [38]. The identity of the mismatched base pairs also had no appreciable impact on the melting temperature.

The melting temperature of probe–target duplex may also be influenced by the fluorophore–quencher pairs. It is well known that most fluorophores and quenchers used to label molecular beacons contain hydrophobic functional groups. When labeled at the ends of molecular beacons, fluorophore–quencher pairs can have hydrophobic interactions if they are in the close proximity. Marras et al. reported an increase of 3 °C in the melting temperature of linear probe–target duplex for Fluorescein–Dabcyl pair and 5 °C for Cy3–Dabcyl pair [39]. A similar effect was observed by Tsourkas et al. [2]. Compared with the values predicted using nearest-neighbor methods, as defined above, an increase of the observed melting temperature was reported.

2.3.1.3 Specificity of Molecular Beacons

Generally, probe specificity is expressed by the difference in melting temperature $\Delta\theta_{\mathrm{m}}$ between the duplex of probe-perfect target and the duplex of probe-mismatched target. For molecular beacons, it has been found that longer stem length results in an improved ability to distinguish between wild-type and mutant targets

over a broader range of temperatures [2, 37]. Molecular beacons with longer stems have better stability in the stem–loop conformation and smaller difference in free energy between closed state and molecular beacon–target duplexes. This generates a reduced binding affinity between single-base mismatched targets and molecular beacons. Tsourkas et al. calculated the fraction of molecular beacon–target duplex at different temperatures for molecular beacons with stems of different lengths and found that $\Delta\theta_m$ increased with the stem length, as shown in Fig. 2.3a [2]. To further evaluate stem length relative to the specificity of molecular beacons in discriminating wild-type and mutant targets, the difference in fraction of probe–target duplex is analyzed. As reported by Tsourkas et al. and shown in Fig. 2.3b below, molecular beacons with 6-base stems were able to discriminate targets over a broader range of temperatures. It was also demonstrated by Tsourkas et al. that molecular beacons with longer probe length had lower specificity.

Specificity and affinity are two major factors that determine the efficiency of nucleic acid probes. In general, sequence specificity and binding affinity of nucleic acid probes are negatively correlated with each other [40, 41]. Figure 2.4 shows the fraction of correct and mismatched complexes for different binding affinities of an oligonucleotide probe. In the graph, a window can be determined where both high affinity and high specificity can be realized. Beyond this window, the specificity decreases, as binding affinity increases. However, because the window of optimal conditions is quite narrow for linear probes, it is highly desirable to find ways to enlarge the optimal range.

Compared with linear probes, one of the most significant advantages of molecular beacons is the higher specificity with which they recognize target sequences [2, 36, 37, 42–44]. The enhanced specificity of molecular beacons is attributed to the three-phase transition of molecular beacons upon interaction with targets, whereas linear nucleic acid probes have only two possible phases: probe–target duplex and random coil. Molecular beacons are capable of forming a hairpin structure that is weaker than the duplex with a correct target, but stronger than the duplex with a mismatched target, as shown in Fig. 2.5 [40, 45, 46].

The enhanced specificity of molecular beacons compared with linear probes can be evaluated by the difference in the complex fraction between probe-wild-type target and probe-mutated target, $\Delta\alpha = \alpha_{WT} - \alpha_{\text{target B}}$ [2, 47]. Compared with linear probes, all molecular beacons with different stem and probe lengths demonstrate an improved ability to discriminate mismatched target (Fig. 2.6). Molecular beacons can not only discriminate between wild-type and mutant targets over a broader range of temperatures, but also maintain a larger difference in fraction of bound molecular beacons between wild-type and mutant targets.

The free energy diagram was also employed to explain the enhanced specificity of molecular beacons [36, 40]. Figure 2.7 shows how molecular beacons can widen the range of optimal conditions for affinity and specificity. In the free energy diagram plotted as a function of temperature, linear probes have an optimal temperature range of $\Delta\theta$, whereas molecular beacons have a much wider range of $\Delta\theta'$. The range is also shifted to lower temperatures where the correct probe–target duplex is more stable. Since molecular beacons are constrained polymers

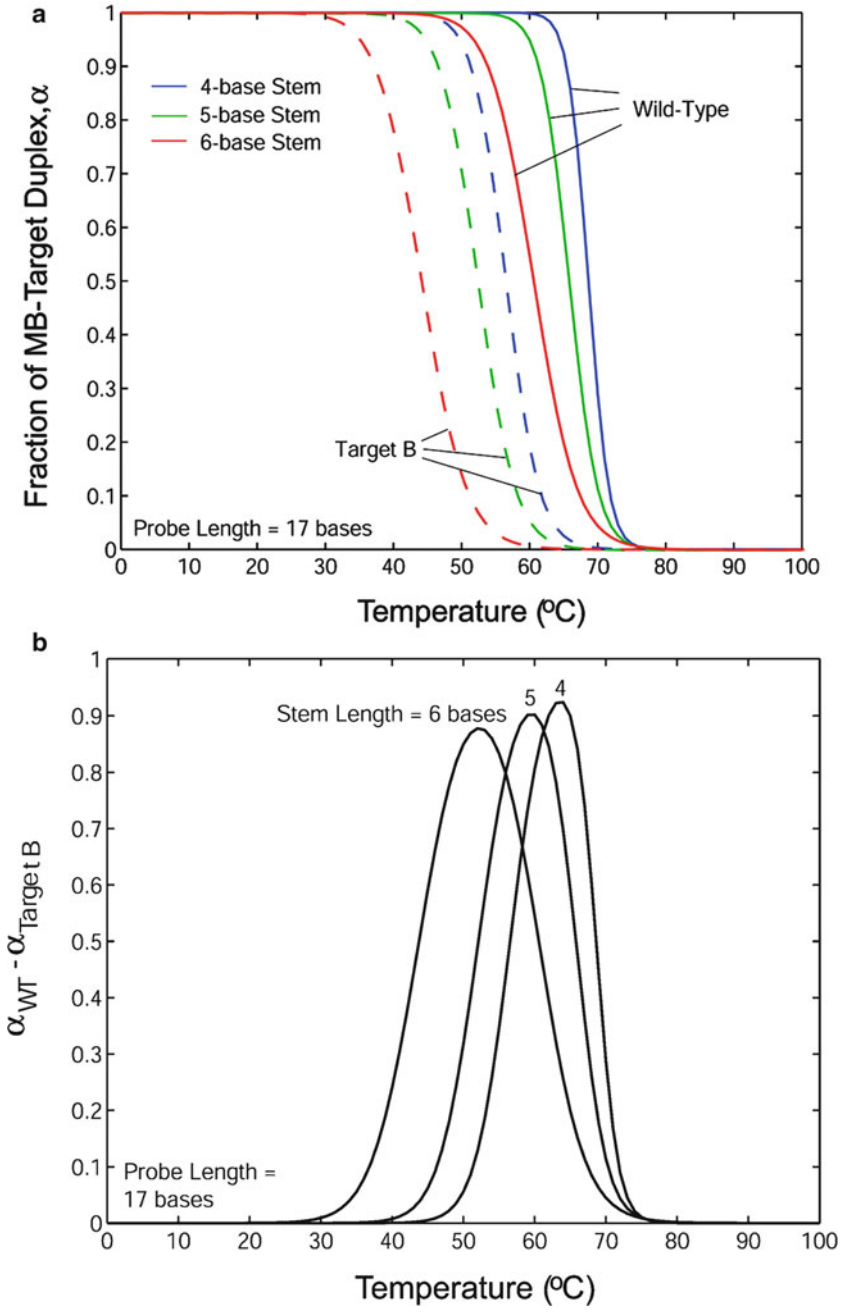

Fig. 2.3 (**a**) Melting curves for molecular beacons hybridizing to wild-type target (*solid line*) and target B (*dashed line*) and (**b**) the difference in the fraction of molecular beacons bound to wild-type target and the fraction of MBs bound to mutant target B. Molecular beacons have a probe length of 17 bases and stem lengths of 4, 5, and 6 bases (Reprinted with the permission from Ref. [2]. Copyright 2003, Oxford University Press, Inc.)

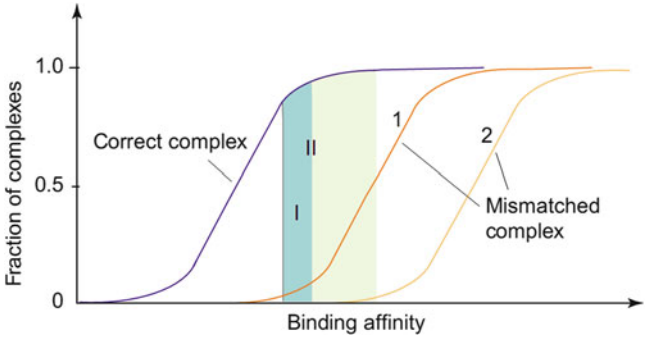

Fig. 2.4 Equilibrium binding of an oligonucleotide probe to correct and mismatched DNA or RNA targets as a function of their binding affinity (Reprinted from Ref. [40], Copyright 2004, with permission from Elsevier)

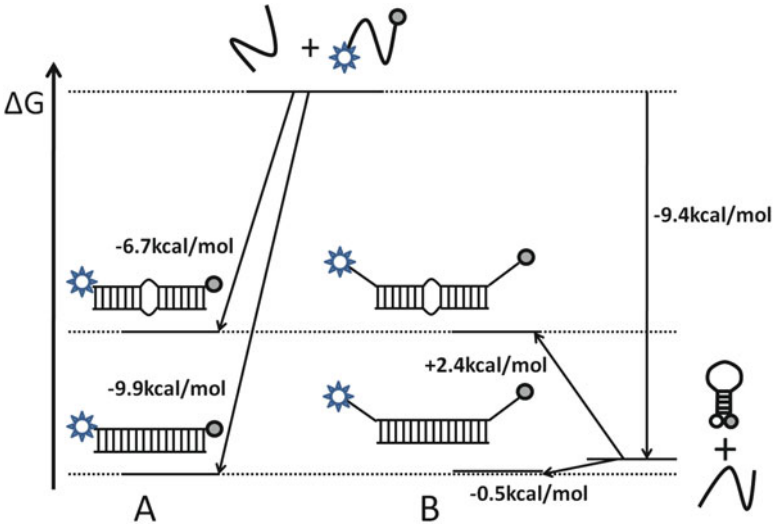

Fig. 2.5 Free energy diagram of hybridization. (**a**) A classical denatured probe of 15 bases; the *two arrows* correspond to the hybridization with a perfect matched target or a one-base-mismatched target. In both cases, complete hybridization takes place, as the free energies are negative. (**b**) A molecular beacon with a loop of 15 bases and a stem of 13 base pairs; in this case, the beacon hybridizes to its perfect matched target (negative free energy), but not to the one-base-mismatched target. The free energy values are calculated according to Eqs. (2.7) and (2.8) found in Sect. 2.3. A schematic of the molecular beacon is shown on the *right* (Reprinted from Ref. [45], Copyright 1999, with permission from Elsevier)

that undergo a greater reorganization than unstructured probes upon formation of probe–target duplexes, they have a better ability to sense a mismatch. Similarly, all conformationally constrained probes should display higher specificity in molecular recognition than unstructured probes.

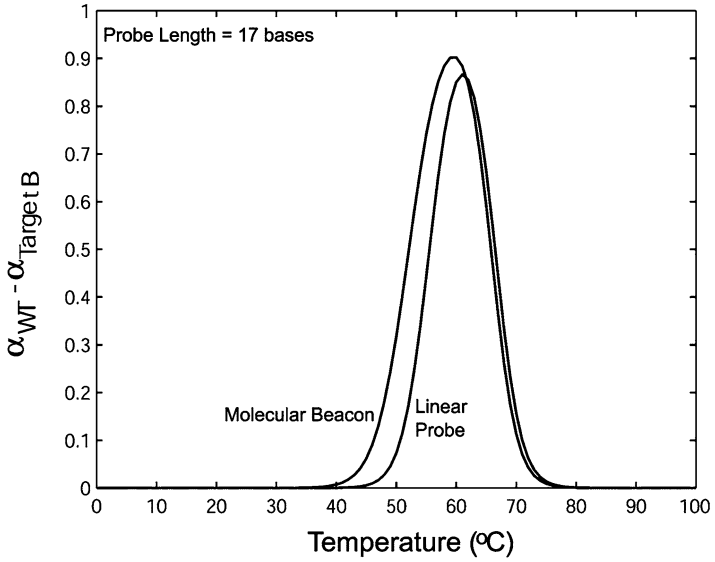

Fig. 2.6 The fraction of molecular beacons compared to the fraction of linear probes bound to wild-type target and mutant target B (Reprinted with the permission from Ref. [2]. Copyright 2003, Oxford University Press, Inc.)

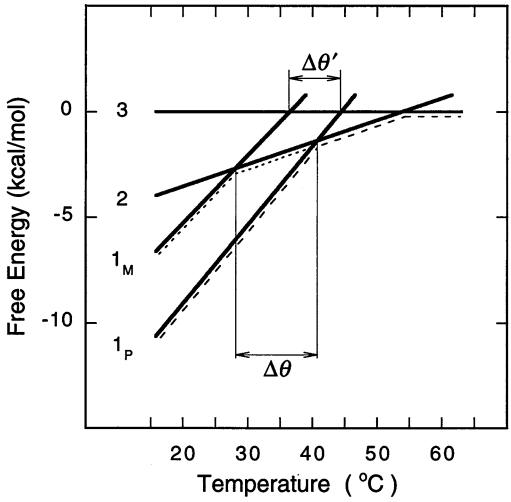

Fig. 2.7 Free energy of the three phases of a solution of molecular beacons in equilibrium with target oligonucleotides. The equation of each line is $\Delta G = \Delta H - \theta \Delta S$. *Straight lines* indicate the free energy of a molecular beacon (curve 2), a linear probe (curve 3), and its duplex complexes with correct (curve 1p) and mismatched (curve 1M) targets (Reprinted with the permission from Ref. [36]. Copyright 1999, National Academy of Sciences, USA)

2.3.1.4 Dynamic Range and Detection Limit

Upon target binding, the three-phase transition of molecular beacons yields different signaling states, and the nonbinding, nonsignaling state is shifted toward the binding, signaling state. Although a larger signal change is induced when the

equilibrium constant is shifted toward the nonbinding state because of the lower background, such signal also reduces the affinity because of a larger conversion of free energy. Thus, similar to other biomolecular switches, the MB's dynamic range and detection limit can be tuned by changing its thermodynamics [48, 49].

As reported by Vallée-Bélisle et al. the three-phase transition model is used to predict the relationship between switching thermodynamics and observed affinities $K_{\mathrm{D}}{}^{\mathrm{obs}}$ by the equation below:

$$K_D^{\mathrm{obs}} = K_D^{\mathrm{int}} \left(\frac{1 + K_{\mathrm{s}}}{K_{\mathrm{s}}} \right) \tag{2.13}$$

where K_D^{int} is the intrinsic affinity of the molecular beacon–target duplex and K_{s} is the switching equilibrium constant from closed hairpin state to random coil [50]. It was found that shifting the equilibrium constant toward the nonbinding state by ten times also increased the dynamic range by ten times which could be done by substituting one A-T with G-C pair in the stem. The upper limit of the dynamic range of concentration could be increased by shifting the equilibrium constant toward the nonbinding state. However, the lowest limits (detection limit) are reached at intermediate values of K_{s}.

2.3.2 Kinetics of Molecular Beacons

The structure of molecular beacons significantly impacts the thermodynamic properties of the molecular beacon–target system, including melting temperature and specificity. Similarly, the kinetics is also influenced by the structure of molecular beacons. For example, longer stems result in slower hybridization kinetics of molecular beacons with target, while molecular beacons with longer loops show larger kinetic constants.

Kinetics information can be obtained by fluorescence measurements [2, 37, 51, 52]. In the analysis of the hybridization kinetics, the association of two oligonucleotides is a second-order reaction, whereas the dissociation is first order, and the reaction can be expressed by the following equation [2]:

$$B + T \underset{k_2}{\overset{k_1}{\rightleftarrows}} D$$

$$\frac{\mathrm{d}[D]}{\mathrm{d}t} = k_1[B][T] - k_2[D] \tag{2.14}$$

where $[B]$, $[T]$, and $[D]$ are the concentrations of molecular beacon, target, and molecular beacon–target complex, respectively, and k_1 and k_2 are the rate constants of formation and dissociation of the molecular beacon–target complex, respectively. The solution of the equation is

$$1 - \frac{[D(t)]}{[D_{eq}]} = e^{-\Delta k_1 t}\left[1 - \lambda \frac{[D(t)]}{[D_{eq}]}\right] \tag{2.15}$$

where $\Delta = \sqrt{(B_0 + T_0 + K_{12})^2 - 4B_0T_0}$, $[D_{eq}] = \frac{1}{2}(B_0 + T_0 + K_{12} - \Delta)$, $\lambda = [D_{eq}]^2 / B_0T_0$, and $K_{12} = k_2/k_1$ is the dissociation constant of the molecular beacon–target duplex. Based on the all-or-nothing assumption, fluorescence intensity of the molecular beacon–target system is proportional to the concentration of molecular beacon–target complex. Thus it can be assumed that

$$\frac{[D(t)]}{[D_{eq}]} = \frac{F(t) - F_0}{F_{eq} - F_0} \tag{2.16}$$

where $F(t)$ is the fluorescence intensity at time t, F_0 is the initial fluorescence intensity, and F_{eq} is the fluorescence intensity at equilibrium. The rate constants k_1 and, subsequently, $k_2 = K_{12}k_1$ were obtained using two methods. Two different curve-fitting methods can be used to obtain the on-rate k_1 and off-rate k_2. One method uses a nonlinear least-square method to fit fluorescence data directly to Eq. (2.15). The second method fits the data to a logarithmic form of Eq. (2.15) with a straight line (the slope is k_1), as shown in this equation:

$$\frac{1}{\Delta}\ln\left(1 - \frac{F(t) - F_0}{F_{eq} - F_0}\right) = \frac{1}{\Delta}\ln\left(1 - \lambda\frac{F(t) - F_0}{F_{eq} - F_0}\right) - k_1 t \tag{2.17}$$

In the example given by Tsourkas et al. the normalized fluorescence restoration was monitored as a function of time after introduction of targets with 17 bases in the loop and four, five, and six bases in the stems. The on-rate constants of molecular beacons with stems and loops of different lengths are plotted and compared. Results showed that molecular beacons always had smaller on-rate constants and that a decrease of stem length significantly increased the on-rate constants. For molecular beacons with 17 bases in the loop, the on-rate constant decreased tenfold when the stem length increased from 5 to 6 bases. Moreover, the probe length can also influence the on-rate constant. Generally, longer probes had faster hybridization kinetics, and this effect was greater for molecular beacons with longer stems.

Different methods have been used to investigate the kinetic properties of DNA hybridization by measuring comparable hybridization/dehybridization rate constants over a wide range of temperature. Based on the results obtained by Chen et al. and Tsourkas et al. a three-step mechanism was proposed to explain the kinetics of hybridization between molecular beacons and targets, as shown in Fig. 2.8b [2, 53, 54]. In the first step, similar with the case of linear probes, the target gets into the close proximity of the probe domain of the hairpin molecular beacon through formation of a few base pairs into a transient intermediate called a nucleus. In the second step, the stem opens along with the formation of more base pairs

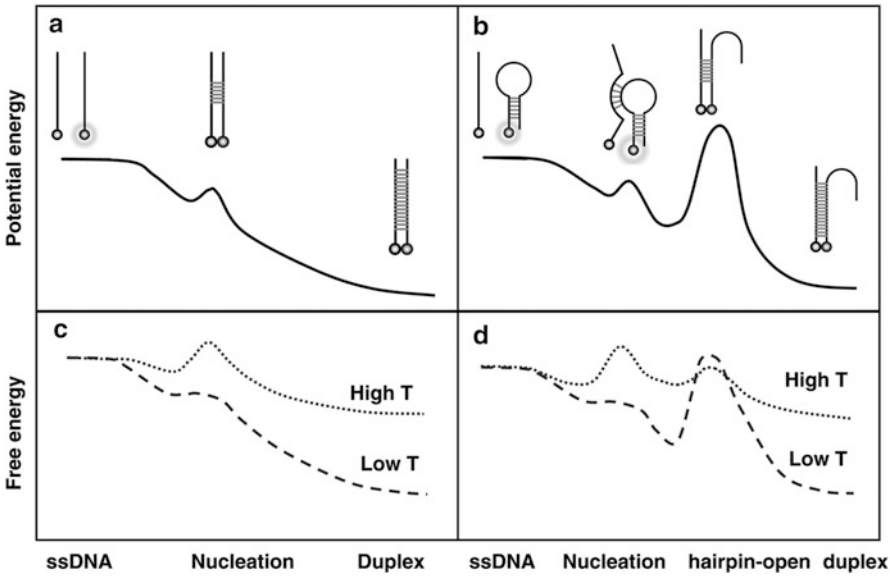

Fig. 2.8 Schematic view of the profiles of potential energy (*solid line*) and free energy at high temperature (*dotted line*) and low temperature (*dashed line*), as a function of reaction progress coordinate for hybridization of random-coil DNA (**a** and **c**) and molecular beacon (**b** and **d**) (Reprinted with the permission from Ref. [54]. Copyright 2007, Oxford University Press, Inc.)

between molecular beacon and target. In the third step, the complete hybridization is achieved after the formation of the remaining base pairs. The rate-limiting step is the first and second step, while the third step is much faster.

Based on standard chemical kinetic theory, a metastable intermediate exists in the rate-limiting step indicated by a negative activation energy for linear probes as shown in Fig. 2.8a [54]. Furthermore, as shown in Fig. 2.8c, at high temperatures, the rate-limiting step is the nucleation of the first few base pairs represented by a negative activation energy. However, at low temperature, the rate-limiting step switches to the diffusion controlled reaction [55, 56]. Compared with the hybridization of linear DNA probes, the hybridization of molecular beacon with target has to overcome one more energy barrier represented by the opening of the hairpin stem (Fig. 2.8b). This free energy barrier decreases as the temperature increases. Therefore, the rate-limiting step switches from the opening of stem to nucleation at high temperatures, as shown in Fig. 2.8d.

In addition, molecular beacons with short stems possess faster binding kinetics with target, while longer stems give a higher energy barrier, resulting in a smaller rate constant in the hybridization process. Molecular beacons with long stems and short probes also show on-rate constants which depend on the probe length because the energy gain in the hybridization of probes barely compensates for the cost for opening the stems.

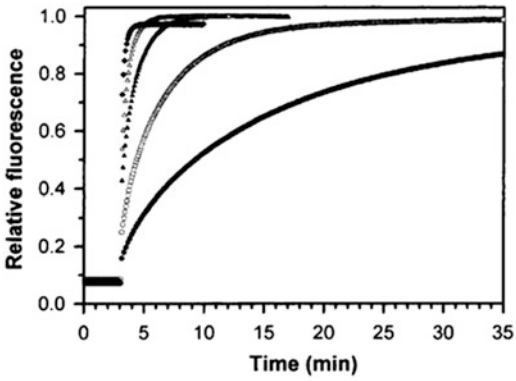

Fig. 2.9 Kinetic responses of molecular beacons upon hybridization to targets at 25 °C in 20 mM Tris–HCl buffer (pH 8.0) containing MgCl2 at different concentrations: 1 (●), 2.5 (○), 5(▲), 10 (△), and 50 mM (♦) (Reprinted with the permission from Ref. [42]. Copyright 2002 American Chemical Society)

2.3.3 Effect of Buffer Conditions on Molecular Beacons

The majority of studies reporting on DNA hybridization were performed in water. Buffer composition has a profound impact on probe performance. Since DNA is a polyanion, it has been reported that a faster hybridization rate could be obtained by increasing the salt concentration [55, 56]. Studies have also reported on DNA hybridization in different organic solvents. McConaughy et al. reported that formamide could accelerate DNA hybridization [57]. It was also reported by Kohne et al. that a water-phenol two-phase system increased the hybridization rate by interfacial adsorption and diffusion [58].

Salt concentration also has an important effect on the hybridization of molecular beacons with targets. Kuhn et al. demonstrated that molecular beacons respond differently to different salt concentrations [42]. Figure 2.9 shows the normalized kinetic responses of molecular beacon–target hybridization at different concentrations of $MgCl_2$. It can be seen that molecular beacons hybridize faster with their targets at higher salt concentrations. Yao et al. [59] reported on the use of immobilized molecular beacons for DNA analysis and observed no fluorescence change in the absence of $MgCl_2$, suggesting that $MgCl_2$ is required for the hybridization of the MB with its target DNA. The fluorescence intensity of an immobilized MB was found to decrease with the increase of $MgCl_2$ concentration from 3 to 200 mM. However, while the fluorescence of the MB–cDNA was enhanced when the $MgCl_2$ concentration was increased from 0 to 100 mM, the fluorescence intensity of MB–cDNA was decreased when the $MgCl_2$ concentration was further increased to 200 mM.

Systematic studies of the effects of different solvents on molecular beacon performance were also carried out. Dave et al. demonstrated DNA detection in nine different organic solvents, each varying up to 75 % (v/v). Compared with DNA detection in water, there are several important features for detection in organic solvents. First, hybridization of the molecular beacon with its target DNA happened in solvent systems containing all nine solvents up to a certain percentage. Second, the hybridization kinetics in most organic solvents was significantly faster than that in water. For example, as shown in Fig. 2.10, the hybridization rate of molecular

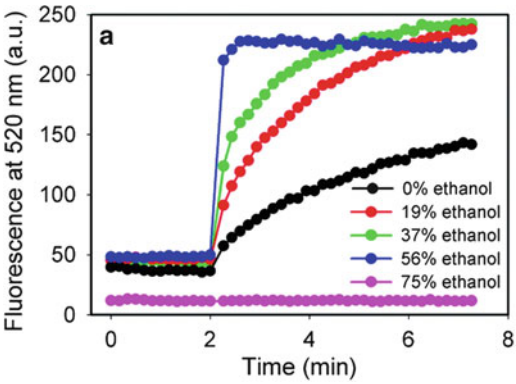

Fig. 2.10 Kinetics of molecular beacon hybridization in 300 mM NaCl and 10 mM HEPES, pH 7.6, with different ethanol percentages (Reprinted with the permission from Ref. [91]. Copyright 2010 American Chemical Society)

beacon with target was enhanced by 70 times in solution with 56 % ethanol. Third, the ability to discriminate single-base mismatch was still maintained in the organic solvent for molecular beacons. Finally, the melting temperature of the molecular beacon–target duplex decreased as the percentage of organic solvents increased.

2.3.4 Optimization of Selectivity and Kinetics of Molecular Beacons

Excellent selectivity is a direct result of hairpin structure and stands out as a major advantage compared to linear probes. Selectivity can be readily improved by optimizing the structure of molecular beacons [2, 44]. From the thermodynamic point of view, the simplest way to improve specificity is to increase the number of base pairs or the G-C content in the stem region. However, although a more stable stem is beneficial to the specificity of molecular beacons, it hinders hybridization kinetics [2]. On the other hand, molecular beacons with short stems have faster hybridization kinetics and improved target affinities, but suffer from a lower signal-to-background ratio and selectivity. The impact of probe length on the behavior of molecular beacons is less significant than that of stem length. Therefore, the selection of the optimal molecular beacon for a specific application appears to be difficult, and a compromise must be found between higher selectivity and faster hybridization. In general, the stem contains about five to seven base pairs, while the loop has 15–25 bases.

Both selectivity and hybridization kinetics are significantly affected by temperature. Therefore, temperature should be considered as an important external factor for designing molecular beacons for certain applications. Higher temperatures drive the opening of molecular beacons to form random coils, generating high background. In order to improve the performance of molecular beacons, especially for applications with relatively high temperatures, alternative strategies have also been developed. First, different from the traditional design of using target-irrelevant

stem, a shared-stem design has been utilized [37]. For this type of molecular beacon, one arm of the stem participates in both stem formation of the closed hairpin and the target hybridization of the opened conformation. This design should be able to improve FRET efficiency based on restricted movement of the dye linked with the shared arm [60]. It also results in higher melting temperatures, as indicated by the thermodynamic studies [37].

Second, different types of synthetic nucleic acids were used to create molecular beacons. For live-cell RNA imaging applications, phosphorothioate DNA [61], 2′-*O*-methyl RNA [47, 62], 2′-*O*-methyl RNA/DNA chimeras [63], peptide nucleic acid (PNA) [42], and locked nucleic acid (LNA) [64, 65] have been employed to construct molecular beacon probes. Nucleic acid affinity for RNA is ranked from highest to lowest: LNA, PNA, 2′-*O*-methyl RNA, RNA, and DNA [66–68]. At first glance, high-affinity probes, by their high melting temperatures, may result in a corresponding high degree of nonspecific hybridization at 37 °C. However, compared with studies performed in solution with high free ion concentrations, studies carried out with fewer ions in the intracellular environment [69, 70] may result in melting temperatures with less effect on hybridization. Therefore, specificity could still be maintained for high-affinity probes in live cells. Tsourkas et al. performed a detailed study of 2′-*O*-methyl and 2′-deoxy molecular beacons in the presence of RNA and DNA targets and found improved stability for 2′-*O*-methyl/RNA duplex accompanied with faster hybridization kinetics [51]. Since LNA–DNA hybridization is stronger than DNA–DNA hybridization, it has also been reported that LNA-molecular beacons are more selective than DNA molecular beacons [71, 72]. As reported by Wang et al. the LNA-MBs remained in a hairpin structure even at 95 °C and had a capability for single nucleotide polymorphism (SNP) detection superior to that of DNA molecular beacons [73].

2.3.5 Surface-Immobilized Molecular Beacons

Microarray technology has made profound contributions to the field of molecular biology with various applications, including pathogen detection, disease diagnostics, gene expression profiling, and drug discovery [74–77]. Surface immobilization of DNA probes allows spatially multiplexed detection, which dramatically accelerates many types of investigation. Compared with linear nucleic acid probes, surface-immobilized molecular beacons possess better specificity and higher signal-to-background ratio.

Comparative studies of DNA hybridization in solution and on solid-solution interface have been performed to analyze the differences in thermodynamic and kinetic properties [78, 79]. It was revealed that hybridization on the solid-solution interface was significantly slower than solution phase and that the hairpin structures in molecular beacon probes further slowed down the hybridization kinetics. Moreover, the traditional model describing the hybridization process in solution phase was not applicable on the solid-solution interface.

In fact, the hybridization of nucleic acid probes with their targets is significantly affected by many factors, such as surface strand density [80], surface charge [81], brush effect [82], point mismatch [83], DNA length [84], and flatness of the substrate [85]. These factors make it necessary to consider the surface interactions between molecular beacons and their targets which are different from those in solution, such as interfacial concentration gradient, probe–interface interactions, and steric hindrance. For example, surface electrostatic interactions greatly affect the binding of surface-immobilized probes with their targets. Nucleic acid targets can be repelled or attracted to the surface depending on the charge of the surface material. Electrostatic repulsion between nucleic acid targets and the surface can block hybridization events. Similarly, steric hindrance caused by increasing probe densities on the surface can further reduce the hybridization efficiency of surface-immobilized probes from repulsive electrostatic interactions.

In general, surface-immobilized molecular beacon probes exhibit lower sensitivities compared with those in solution. The lower sensitivity is partially attributed to the inefficient quenching of the molecular beacons on the surface caused by their nonspecific interactions with the supporting materials. These interactions tend to destabilize the hairpin structures of molecular beacons. Glass has been widely used as a solid support for the immobilization of MBs [59, 86]. Unfortunately, glass suffers from interfacial effect of static charging which partially opens molecular beacons, resulting in high background signals for the immobilized molecular beacons in the absence of targets. Molecular beacons have also been immobilized on porous surfaces using hydrogel films, which create a solution-like environment [87]. However, the gel network slows down the hybridization process by restricted transport of targets. Gold surfaces have also been employed as substrates for immobilization of molecular beacons as a consequence of the easy chemistry linkage, as well as the fluorescence quenching ability, of gold [88, 89]. However, nitrogen-based functional groups on DNA bases can be nonspecifically adsorbed to the gold surfaces through chemical adsorption [88]. Another issue concerning molecular beacons immobilized on gold surfaces is the nonuniform distribution of probes which affects sensitivity, specificity, and kinetics [88, 90].

2.4 Summary

Molecular beacon probes with high specificity and sensitivity have become an important tool in biomedical and bioanalytical studies. The advantages of molecular beacons are attributed to the flexible stem–loop hairpin structures. The conformational fluctuations of molecular beacons in the absence of targets can be described using the equilibrium between the open and closed states. In the presence of targets, the interaction between molecular beacons and targets is characterized by a three-phase model: hybridized with a target, free in the stem–loop conformation, and free as a random coil. The thermodynamics and kinetics of molecular beacons are mainly determined by their hairpin structures and sequences, but can be equally

affected by many other factors, such as temperature, salt concentration, solvents, and probe–surface interactions. To optimize the performance of molecular beacons, factors that affect affinity, specificity, and kinetics must be considered and a probe design and experimental conditions carefully chosen on the basis of the purpose of different applications.

References

1. Tyagi S, Kramer FR (1996) Molecular beacons: probes that fluoresce upon hybridization. Nat Biotechnol 14:303–308
2. Tsourkas A, Behlke MA, Rose SD, Bao G (2003) Hybridization kinetics and thermodynamics of molecular beacons. Nucleic Acids Res 31:1319–1330
3. Bonnet G, Krichevsky O, Libchaber A (1998) Kinetics of conformational fluctuations in DNA hairpin-loops. Proc Natl Acad Sci U S A 95:8602–8606
4. Vallone PM, Benight AS (1999) Melting studies of short DNA hairpins containing the universal base 5-nitroindole. Nucleic Acids Res 27:3589–3596
5. Antao VP, Tinoco I (1992) Thermodynamic parameters for loop formation in RNA and DNA hairpin tetraloops. Nucleic Acids Res 20:819–824
6. Vallone PM, Paner TM, Hilario J, Lane MJ, Faldasz BD, Benight AS (1999) Melting studies of short DNA hairpins: influence of loop sequence and adjoining base pair identity on hairpin thermodynamic stability. Biopolymers 50:425–442
7. Rentzeperis D, Shikiya R, Maiti S, Ho J, Marky LA (2002) Folding of intramolecular DNA hairpin loops: enthalpy-entropy compensations and hydration contributions. J Phys Chem B 106:9945–9950
8. Breslauer KJ, Frank R, Blöcker H, Marky LA (1986) Predicting DNA duplex stability from the base sequence. Proc Natl Acad Sci U S A 83:3746–3750
9. SantaLucia J (1998) A unified view of polymer, dumbbell, and oligonucleotide DNA nearest-neighbor thermodynamics. Proc Natl Acad Sci U S A 95:1460–1465
10. Owczarzy R, Vallone PM, Gallo FJ, Paner TM, Lane MJ, Benight AS (1997) Predicting sequence-dependent melting stability of short duplex DNA oligomers. Biopolymers 44:217–239
11. Jaeger JA, Turner DH, Zuker M (1989) Improved predictions of secondary structures for RNA. Proc Natl Acad Sci U S A 86:7706–7710
12. Haasnoot C, De Bruin S, Berendsen R, Janssen H, Binnendijk T, Hilbers C, Van der Marel G, Van Boom J (1983) Structure, kinetics and thermodynamics of DNA hairpin fragments in solution. J Biomol Struct Dyn 1:115–129
13. Haasnoot CA, Hilbers CW, van der Marel GA, van Boom JH, Singh UC, Pattabiraman N, Kollman PA (1986) On loop folding in nucleic acid hairpin-type structures. J Biomol Struct Dyn 3:843–857
14. Tinoco I, Borer PN, Dengler B, Levine MD, Uhlenbeck OC, Crothers DM, Gralla J (1973) Improved estimation of secondary structure in ribonucleic acids. Nature 246:40–41
15. Senior MM, Jones RA, Breslauer KJ (1988) Influence of loop residues on the relative stabilities of DNA hairpin structures. Proc Natl Acad Sci U S A 85:6242–6246
16. Schildkraut C, Lifson S (1965) Dependence of the melting temperature of DNA on salt concentration. Biopolymers 3:195–208
17. Owczarzy R, You Y, Moreira BG, Manthey JA, Huang L, Behlke MA, Walder JA (2004) Effects of sodium ions on DNA duplex oligomers: improved predictions of melting temperatures. Biochemistry (NY) 43:3537–3554
18. Tan ZJ, Chen SJ (2006) Nucleic acid helix stability: effects of salt concentration, cation valence and size, and chain length. Biophys J 90:1175–1190

19. Tan ZJ, Chen SJ (2007) RNA helix stability in mixed Na/Mg_2 solution. Biophys J 92:3615–3632
20. Tan ZJ, Chen SJ (2008) Salt dependence of nucleic acid hairpin stability. Biophys J 95:738–752
21. Turner D, Sugimoto N, Freier S (1990) Thermodynamics and kinetics of base-pairing and of DNA and RNA self-assembly and helix coil transition. Nucleic Acids 1:201–227
22. Bloomfield VA, Crothers DM, Tinoco I (2000) Nucleic acids: structures, properties, and functions. University Science Books, Sausalito
23. Ansari A, Kuznetsov SV, Shen Y (2001) Configurational diffusion down a folding funnel describes the dynamics of DNA hairpins. Proc Natl Acad Sci U S A 98:7771–7776
24. Shen Y, Kuznetsov SV, Ansari A (2001) Loop dependence of the dynamics of DNA hairpins. J Phys Chem B 105:12202–12211
25. Kuznetsov SV, Shen Y, Benight AS, Ansari A (2001) A semiflexible polymer model applied to loop formation in DNA hairpins. Biophys J 81:2864–2875
26. Bevilacqua PC, Blose JM (2008) Structures, kinetics, thermodynamics, and biological functions of RNA hairpins. Annu Rev Phys Chem 59:79–103
27. Wallace MI, Ying L, Balasubramanian S, Klenerman D (2001) Non-Arrhenius kinetics for the loop closure of a DNA hairpin. Proc Natl Acad Sci U S A 98:5584–5589
28. Wallace MI, Ying L, Balasubramanian S, Klenerman D (2000) FRET fluctuation spectroscopy: exploring the conformational dynamics of a DNA hairpin loop. J Phys Chem B 104:11551–11555
29. Wemmer DE, Chou SH, Hare DR, Reid BR (1985) Duplex-hairpin transitions in DNA: NMR studies on CGCGTATACGCG. Nucleic Acids Res 13:3755–3772
30. Youil R, Kemper BW, Cotton R (1995) Screening for mutations by enzyme mismatch cleavage with T4 endonuclease VII. Proc Natl Acad Sci U S A 92:87–91
31. Nelson NC, Hammond PW, Matsuda E, Goud AA, Becker MM (1996) Detection of all single-base mismatches in solution by chemiluminescence. Nucleic Acids Res 24:4998–5003
32. Dubertret B, Calame M, Libchaber AJ (2001) Single-mismatch detection using gold-quenched fluorescent oligonucleotides. Nat Biotechnol 19:365–370
33. Kostrikis LG, Tyagi S, Mhlanga MM, Ho DD, Kramer FR (1998) Spectral genotyping of human alleles. Science 279:1228–1229
34. Marras SAE, Russell Kramer F, Tyagi S (1999) Multiplex detection of single-nucleotide variations using molecular beacons. Genet Anal Biomol Eng 14:151–156
35. Meroueh M, Chow CS (1999) Thermodynamics of RNA hairpins containing single internal mismatches. Nucleic Acids Res 27:1118–1125
36. Bonnet G, Tyagi S, Libchaber A, Kramer FR (1999) Thermodynamic basis of the enhanced specificity of structured DNA probes. Proc Natl Acad Sci U S A 96:6171–6176
37. Tsourkas A, Behlke MA, Bao G (2002) Structure–function relationships of shared-stem and conventional molecular beacons. Nucleic Acids Res 30:4208–4215
38. Cantor CR (1980) Biophysical chemistry: Part III: The behavior of biological macromolecules. WH Freeman & Co, San Francisco
39. Marras SAE, Kramer FR, Tyagi S (2002) Efficiencies of fluorescence resonance energy transfer and contact-mediated quenching in oligonucleotide probes. Nucleic Acids Res 30:e122
40. Demidov VV, Frank-Kamenetskii MD (2004) Two sides of the coin: affinity and specificity of nucleic acid interactions. Trends Biochem Sci 29:62–71
41. Lomakin A, Frank-Kamenetskii MD (1998) A theoretical analysis of specificity of nucleic acid interactions with oligonucleotides and peptide nucleic acids (PNAs). J Mol Biol 276:57–70
42. Kuhn H, Demidov VV, Coull JM, Fiandaca MJ, Gildea BD, Frank-Kamenetskii M (2002) Hybridization of DNA and PNA molecular beacons to single-stranded and double-stranded DNA targets. J Am Chem Soc 124:1097–1103
43. Tan L, Li Y, Drake TJ, Moroz L, Wang K, Li J, Munteanu A, Yang CJ, Martinez K, Tan W (2005) Molecular beacons for bioanalytical applications. Analyst 130:1002–1005
44. Goel G, Kumar A, Puniya A, Chen W, Singh K (2005) Molecular beacon: a multitask probe. J Appl Microbiol 99:435–442
45. Bonnet G, Libchaber A (1999) Optimal sensitivity in molecular recognition. Phys A 263:68–77

46. Wang K, Tang Z, Yang CJ, Kim Y, Fang X, Li W, Wu Y, Medley CD, Cao Z, Li J (2009) Molecular engineering of DNA: molecular beacons. Angew Chem Int Ed 48:856–870
47. Bratu DP, Cha BJ, Mhlanga MM, Kramer FR, Tyagi S (2003) Visualizing the distribution and transport of mRNAs in living cells. Proc Natl Acad Sci U S A 100:13308–13313
48. Beisel CL, Bayer TS, Hoff KG, Smolke CD (2008) Model-guided design of ligand-regulated RNAi for programmable control of gene expression. Mol Syst Biol 4:224
49. Kim JR, Ostermeier M (2006) Modulation of effector affinity by hinge region mutations also modulates switching activity in an engineered allosteric TEM1 [beta]-lactamase switch. Arch Biochem Biophys 446:44–51
50. Vallée-Bélisle A, Ricci F, Plaxco KW (2009) Thermodynamic basis for the optimization of binding-induced biomolecular switches and structure-switching biosensors. Proc Natl Acad Sci U S A 106:13802–13807
51. Tsourkas A, Behlke MA, Bao G (2002) Hybridization of 2′-O-methyl and 2′-deoxy molecular beacons to RNA and DNA targets. Nucleic Acids Res 30:5168–5174
52. Yao G, Fang X, Yokota H, Yanagida T, Tan W (2003) Monitoring molecular beacon DNA probe hybridization at the single-molecule level. Chem Eur J 9:5686–5692
53. Nakano S, Kirihata T, Fujii S, Sakai H, Kuwahara M, Sawai H, Sugimoto N (2007) Influence of cationic molecules on the hairpin to duplex equilibria of self-complementary DNA and RNA oligonucleotides. Nucleic Acids Res 35:486–494
54. Chen C, Wang W, Wang Z, Wei F, Zhao XS (2007) Influence of secondary structure on kinetics and reaction mechanism of DNA hybridization. Nucleic Acids Res 35:2875–2884
55. Porschke D, Eigen M (1971) Co-operative non-enzymatic base recognition III. Kinetics of the helix–coil transition of the oligoribouridylic · oligoriboadenylic acid system and of oligoriboadenylic acid alone at acidic pH. J Mol Biol 62:361–364
56. Pörschke D, Uhlenbeck O, Martin F (1973) Thermodynamics and kinetics of the helix-coil transition of oligomers containing GC base pairs. Biopolymers 12:1313–1335
57. McConaughy BL, Laird CD, McCarthy BJ (1969) Nucleic acid reassociation in formamide. Biochemistry (NY) 8:3289–3295
58. Kohne DE, Levison SA, Byers MJ (1977) Room temperature method for increasing the rate of DNA reassociation by many thousandfold: the phenol emulsion reassociation technique. Biochemistry (NY) 16:5329–5341
59. Yao G, Tan W (2004) Molecular-beacon-based array for sensitive DNA analysis. Anal Biochem 331:216–223
60. Tsourkas A, Bao G (eds) (2001) Detecting mRNA transcripts using FRET-enhanced molecular beacons. ASME BED
61. Vijayanathan V, Thomas T, Sigal LH, Thomas T (2002) Direct measurement of the association constant of HER2/neu antisense oligonucleotide to its target RNA sequence using a molecular beacon. Antisense Nucleic Acid Drug Dev 12:225–233
62. Mhlanga MM, Vargas DY, Fung CW, Kramer FR, Tyagi S (2005) tRNA-linked molecular beacons for imaging mRNAs in the cytoplasm of living cells. Nucleic Acids Res 33:1902–1912
63. Santangelo PJ, Bao G (2007) Dynamics of filamentous viral RNPs prior to egress. Nucleic Acids Res 35:3602–3611
64. Martinez K, Estevez M, Wu Y, Phillips JA, Medley CD, Tan W (2009) Locked nucleic acid based beacons for surface interaction studies and biosensor development. Anal Chem 81:3448–3454
65. Wu Y, Yang CJ, Moroz LL, Tan W (2008) Nucleic acid beacons for long-term real-time intracellular monitoring. Anal Chem 80:3025–3028
66. Vester B, Wengel J (2004) LNA (locked nucleic acid): high-affinity targeting of complementary RNA and DNA. Biochemistry (NY) 43:13233–13241
67. Kurreck J, Wyszko E, Gillen C, Erdmann VA (2002) Design of antisense oligonucleotides stabilized by locked nucleic acids. Nucleic Acids Res 30:1911–1918
68. Aartsma-Rus A, Kaman W, Bremmer-Bout M, Janson A, Den Dunnen J, van Ommen GJB, van Deutekom J (2004) Comparative analysis of antisense oligonucleotide analogs for targeted DMD exon 46 skipping in muscle cells. Gene Ther 11:1391–1398

69. Romani A (2007) Regulation of magnesium homeostasis and transport in mammalian cells. Arch Biochem Biophys 458:90–102
70. Santangelo PJ (2010) Molecular beacons and related probes for intracellular RNA imaging. Wiley Interdiscip Rev Nanomed Nanobiotechnol 2:11–19
71. Koshkin AA, Nielsen P, Meldgaard M, Rajwanshi VK, Singh SK, Wengel J (1998) LNA (locked nucleic acid): an RNA mimic forming exceedingly stable LNA: LNA duplexes. J Am Chem Soc 120:13252–13253
72. Koshkin AA, Singh SK, Nielsen P, Rajwanshi VK, Kumar R, Meldgaard M, Olsen CE, Wengel J (1998) LNA (locked nucleic acids): synthesis of the adenine, cytosine, guanine, 5-methylcytosine, thymine and uracil bicyclonucleoside monomers, oligomerisation, and unprecedented nucleic acid recognition. Tetrahedron 54:3607–3630
73. Wang L, Yang CJ, Medley CD, Benner SA, Tan W (2005) Locked nucleic acid molecular beacons. J Am Chem Soc 127:15664–15665
74. Yoo SM, Keum KC, Yoo SY, Choi JY, Chang KH, Yoo NC, Yoo WM, Kim JM, Lee D, Lee SY (2004) Development of DNA microarray for pathogen detection. Biotechnol Bioprocess Eng 9:93–99
75. Gracey AY, Cossins AR (2003) Application of microarray technology in environmental and comparative physiology. Annu Rev Physiol 65:231–259
76. Fan J, Yang X, Wang W, Wood WH, Becker KG, Gorospe M (2002) Global analysis of stress-regulated mRNA turnover by using cDNA arrays. Proc Natl Acad Sci U S A 99:10611–10616
77. Fang Y, Frutos AG, Lahiri J (2003) Ganglioside microarrays for toxin detection. Langmuir 19:1500–1505
78. Sekar M, Bloch W, St John PM (2005) Comparative study of sequence-dependent hybridization kinetics in solution and on microspheres. Nucleic Acids Res 33:366–375
79. Gao Y, Wolf LK, Georgiadis RM (2006) Secondary structure effects on DNA hybridization kinetics: a solution versus surface comparison. Nucleic Acids Res 34:3370–3377
80. Peterson AW, Heaton RJ, Georgiadis RM (2001) The effect of surface probe density on DNA hybridization. Nucleic Acids Res 29:5163–5168
81. Vainrub A, Montgomery Pettitt B (2003) Surface electrostatic effects in oligonucleotide microarrays: control and optimization of binding thermodynamics. Biopolymers 68:265–270
82. Halperin A, Buhot A, Zhulina E (2005) Brush effects on DNA chips: thermodynamics, kinetics, and design guidelines. Biophys J 89:796–811
83. Tawa K, Knoll W (2004) Mismatching base-pair dependence of the kinetics of DNA–DNA hybridization studied by surface plasmon fluorescence spectroscopy. Nucleic Acids Res 32:2372–2377
84. Stillman BA, Tonkinson JL (2001) Expression microarray hybridization kinetics depend on length of the immobilized DNA but are independent of immobilization substrate. Anal Biochem 295:149–157
85. Glazer MI, Fidanza JA, McGall GH, Trulson MO, Forman JE, Frank CW (2007) Kinetics of oligonucleotide hybridization to DNA probe arrays on high-capacity porous silica substrates. Biophys J 93:1661–1676
86. Liu X, Tan W (1999) A fiber-optic evanescent wave DNA biosensor based on novel molecular beacons. Anal Chem 71:5054–5059
87. Wang H, Li J, Liu H, Liu Q, Mei Q, Wang Y, Zhu J, He N, Lu Z (2002) Label-free hybridization detection of a single nucleotide mismatch by immobilization of molecular beacons on an agarose film. Nucleic Acids Res 30:e61
88. Du H, Strohsahl CM, Camera J, Miller BL, Krauss TD (2005) Sensitivity and specificity of metal surface-immobilized molecular beacon biosensors. J Am Chem Soc 127:7932–7940
89. Du H, Disney MD, Miller BL, Krauss TD (2003) Hybridization-based unquenching of DNA hairpins on Au surfaces: prototypical “molecular beacon” biosensors. J Am Chem Soc 125:4012–4013
90. Sauthier ML, Carroll RL, Gorman CB, Franzen S (2002) Nanoparticle layers assembled through DNA hybridization: characterization and optimization. Langmuir 18:1825–1830
91. Dave N, Liu J (2010) Fast molecular beacon hybridization fast molecular bea-con hybridization. J Phys Chem B 114:15694–15699

http://www.springer.com/978-3-642-39109-5

Molecular Beacons
Yang, C.J.; Tan, W. (Eds.)
2013, IX, 194 p. 88 illus., 70 illus. in color.,
ISBN: 978-3-642-39109-5